International Journal of Pharmaceutics 401 (2010) 103–112

Contents lists available at ScienceDirect

International Journal of Pharmaceutics

journal homepage: www.elsevier.com/locate/ijpharm

Pharmaceutical Nanotechnology

PEGylation and preliminary biocompatibility evaluation of magnetite–silica nanocomposites obtained by high energy ball milling

Martina Pilloni[a,b], Julien Nicolas[a,*], Véronique Marsaud[a], Kawthar Bouchemal[a], Francesca Frongia[b], Alessandra Scano[c], Guido Ennas[b], Catherine Dubernet[a]

[a] Laboratoire de Physico-Chimie, Pharmacotechnie et Biopharmacie, Univ Paris-Sud, UMR CNRS 8612, Faculté de Pharmacie, 5 rue Jean-Baptiste Clément, F-92296 Châtenay-Malabry Cedex, France
[b] Dipartimento di Scienze Chimiche, Universita' di Cagliari, 09042 Monserrato (CA), Italy
[c] Asociación Industria Navarra (AIN), Centro de Ingeniería Avanzada de Superficies, San Cosme y San Damián, s/n 31191 Cordovilla, Pamplona, Spain

ARTICLE INFO

Article history:
Received 4 June 2010
Received in revised form 2 September 2010
Accepted 14 September 2010
Available online 18 September 2010

Keywords:
Magnetite–silica nanocomposites
High energy ball milling
PEGylation
Protein interaction
Cytotoxicity

ABSTRACT

High energy ball milling (HEBM) has been used for the first time to prepare PEGylated magnetite–silica (Fe_3O_4–SiO_2) nanocomposites intended to be used for biological purposes. Surface amine groups were introduced by a silanization reaction involving 3-aminopropyl triethoxysilane (APTS) followed by PEGylation to yield long-term stable and stealth nanocomposites of 200 nm in diameter. The efficient coverage by PEG chains was shown by isothermal titration calorimetry (ITC) where PEGylated nanocomposites did not interact with BSA compared to non-PEGylated counterparts which led to a significant change in enthalpy. By cell viability (MTT) assays and cell morphology investigations, it was evidenced that PEGylated Fe_3O_4–SiO_2 nanocomposites did not provide any appreciable cytotoxicity on J774 macrophage and MCF-7 breast cancer cell lines. Furthermore, noticeable internalization was evidenced by J774 cells with PEGylated Fe_3O_4–SiO_2 nanocomposites in contrast to MCF-7 cells, in good agreement with the respective tendency of each cell line for endocytosis.

1. Introduction

Over the last years, magnetic iron oxide nanoparticles have appeared as a well-established technology and an important research field due to the superparamagnetism of those colloidal materials allowing them to be guided with an external magnetic field (Laurent et al., 2008). This approach recently opened the door to a wide range of potential applications in the field of biotechnology and nanomedicine such as biomagnetic separations, biosensors, carriers for targeted drug delivery and contrast agents in magnetic resonance imaging (Di Marco et al., 2007; Laurent et al., 2008; Na et al., 2009; Neuberger et al., 2005; Sajja et al., 2009; Teja and Koh, 2009).

However, the direct use of magnetic particles for biomedical assays is not possible due to the formation of large aggregates which tend to: (i) lose their high magnetization due to oxidation and (ii) undertake rapid clearance due to their prompt recognition by the immune system (Kobayashi et al., 2008). To circumvent these strong limitations, a practical solution consists in the coating of the magnetic part with an inert host material such as silica (the resulting materials are usually termed magnetite–silica or iron oxide–silica nanocomposites) in order to provide a high colloidal stability in aqueous solution over a broad range of pH and to keep the magnetic properties, thus making them promising candidates for biomedical applications (Sun et al., 2004). Besides, the presence of silanol moieties can easily react with various coupling agents to covalently attach specific ligands, thus representing an avenue for active cell targeting (Laurent et al., 2008).

To the best of our knowledge, three different synthetic routes have been investigated for the preparation of magnetic silica nanoparticles so far (Laurent et al., 2008). The first method is based on the well-known sol–gel approach (Solinas et al., 2001), which relies on the Stöber process (Stöber et al., 1968), and has proven to be a robust pathway to generate magnetic nanocomposites due to strong surface affinity of magnetite for silica (Barnakov et al., 2005, Deng et al., 2005; Im et al., 2005; Lu et al., 2002; Philipse and van Bruggen, 1994). The second method consists in the deposition of silica from silicic acid solution which appeared to be more efficient regarding the covering efficiency of the magnetite surface than the sol–gel approach (Butterworth et al., 1996; Liu et al., 2004b). The third method employs (inverse) micelles to confine and control the silica coating but requires an additional purification step in order to remove the large amount of surfactant from the nanocomposites (Gao et al., 2003; Philipse and van Bruggen, 1994; Tartaj and Serna, 2002, 2003).

* Corresponding author. Tel.: +33 1 46 83 58 53; fax: +33 1 46 83 59 46.
E-mail address: julien.nicolas@u-psud.fr (J. Nicolas).

0378-5173/$ – see front matter © 2010 Elsevier B.V. All rights reserved.
doi:10.1016/j.ijpharm.2010.09.010

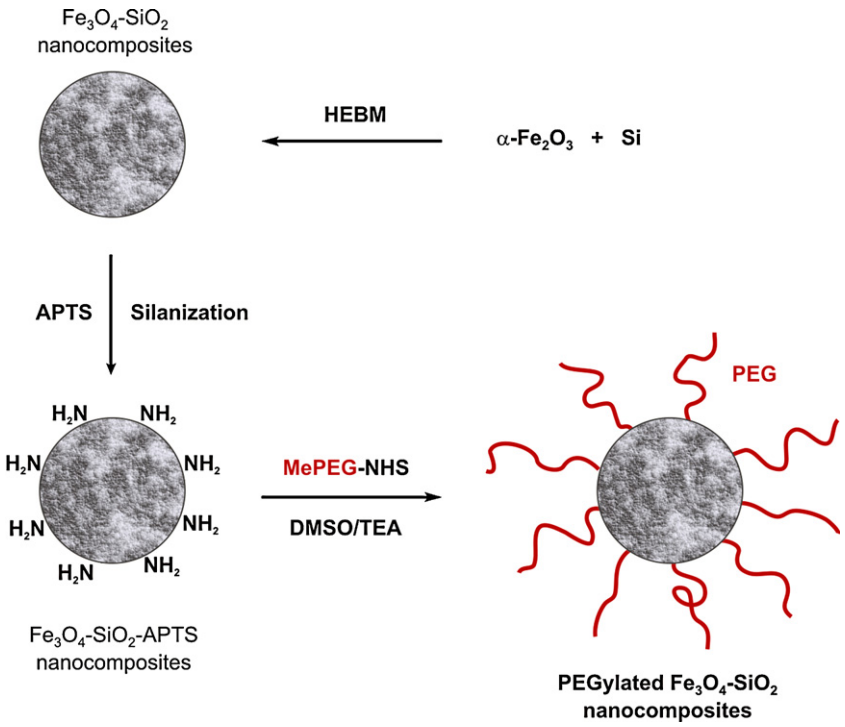

Scheme 1. Synthesis of PEGylated Fe_3O_4–SiO_2 nanocomposites by high energy ball milling followed by silanization and PEGylation.

Herein, we propose a "solid state method", namely high energy ball milling (HEBM), as a novel approach to obtain nanometer-sized magnetite–silica nanocomposites intended to be used for biological purposes (Scheme 1). This technique is believed to be an interesting alternative to the above-cited routes from both a practical and an economical point of view. Indeed, HEBM has been initially developed in the 70s as an industrial process to successfully produce new alloys and composites (Kong et al., 2008). In nanomaterials research area, several attempts have been undertaken with this top down approach to produce materials at the nanoscale (Castrillo et al., 2007; Ishida and Tamaru, 1993; Sorrentino et al., 2005; Zhu et al., 2006), but none of them reported the synthesis of magnetite–silica nanocomposites.

In this work, surface engineering was also performed for further attachment of reactive poly(ethylene glycol) chains, the so-called PEGylation (Veronese, 2001), in order to improve colloidal stability and to confer stealth properties to these nanocomposites (Scheme 1). Indeed, it is well-admitted that PEG gives rise to several potential beneficial effects including increased bioavailability and plasma half-lives, biocompatibility/decreased immunogenicity, reduced proteolysis, and enhanced stability (Roberts et al., 2002, Stolnik et al., 1995; Veronese, 2001; Veronese and Harris, 2002). Besides, in order to have a deeper insight into our magnetite–silica nanocomposites, preliminary cytotoxicity studies and protein interaction measurements via isothermal titration calorimetry (ITC) will be performed and discussed.

2. Materials and methods

2.1. Materials

2-Propanol (99.5%), dichloromethane (DCM), anhydrous magnesium sulfate ($MgSO_4$, >99%), 4-dimethylaminopyridine (DMAP, 99%), anhydrous dimethyl sulfoxide (DMSO, 99.9%), triethyl amine (TEA), 3-aminopropyl triethoxysilane (APTS, ≥99%) and *N*-hydroxysuccinimide (NHS, 98%) were all purchased from Aldrich and used as received. Poly(ethylene glycol) monomethyl ether (MePEG, M_n = 2000 g mol^{-1}), *N*,*N*-dicyclohexylcarbodiimide (DCC, >99%) and ammonium hydroxide (>99.99%) were purchased from Fluka and used without further purification. Hematite (α-Fe_2O_3, Carlo Erba, 99.9%) and silicon (Fluka 99.9%) were used as received. Solvents were purchased at the highest grade from Carlo Erba.

2.2. Synthesis of magnetite–silica nanocomposites and functionalization procedures

2.2.1. Synthesis of magnetite–silica nanocomposites by HEBM

The synthesis of nanocomposite was carried out by a high-energy ball milling (HEBM) technique starting from a mixture of α-Fe_2O_3 and silicon powder according to the following equation: $6\alpha\text{-}Fe_2O_3 + Si \rightarrow 4Fe_3O_4 + SiO_2$ (Scano et al., submitted for publication). The composition of the reaction mixture was selected as to obtain a final content of 6 wt.% of SiO_2 within the nanocomposites. Briefly, a mixture of α-Fe_2O_3 (1.36 g) and Si (0.04 g) was sealed in a 60 mL stainless steel vial with balls from the same material (70 g, 6.35 nm in diameter) under argon atmosphere to avoid contact with oxygen. In order to prevent overheating of the vial, the milling was carried out following consecutive milling (Spex 8000 vibratory mill, Spex CertiPrep, Metuchen, NJ) and rest periods (5 min). The milling was monitored by X-ray powder diffraction (XRD) at different milling times. Milling was interrupted after 4 h and the sample (Fe_3O_4–SiO_2) was collected.

2.2.2. Functionalization of magnetite–silica nanocomposites by APTS

Magnetite–silica nanocomposites were then functionalized with 3-aminopropyl triethoxysilane (APTS) by a silanization reaction adapted from del Campo et al. (2005). In a typical procedure, an aqueous suspension of nanocomposites with APTS (5 mL) was heated at 75 °C by means of a water bath. The pH of the suspension was slightly acidic (by addition of hydrochloric acid) to promote APTS hydrolysis. After 1 h, the pH was adjusted to 9 with ammonium hydroxide and the temperature was increased up to 90 °C until complete dryness. The resulting product was washed with dis-

tilled water and acetone, and then dried at 40 °C under high vacuum until constant weight to yield the Fe_3O_4–SiO_2–APTS powder.

2.3. Synthesis of methoxypoly(ethylene glycol) N-succinimidyl ester (MePEG-NHS)

2.3.1. Synthesis of methoxypoly(ethylene glycol) monocarboxylic acid (MePEG-COOH)

In a 100 mL round bottom flask, poly(ethylene glycol) monomethyl ether (5 g, 2.5×10^{-3} mol) was dissolved in acetone (60 mL) and reacted with Jones Reagent (2.8 mL) overnight at room temperature under magnetic stirring (Lele and Kulkarni, 1998). The reaction was stopped by adding 2-propanol (5 mL) and the resulting chromium salts precipitate was removed by passing the reaction medium through activated charcoal (2 g). The resulting colourless solution was then evaporated under reduced pressure. The solid was dissolved in DCM and washed with multiple portions of aqueous 1 M HCl solution. The organic phase was dried over $MgSO_4$, filtered off and dried under high vacuum to give a fine, white powder in a quantitative fashion. ^{1}H NMR ($CDCl_3$) δ = 3.37 (s, 3H, OCH_3), 3.45–3.95 (m, 190H, OCH_2CH_2O), 4.15 (s, 2H, CH_2COOH).

2.3.2. Synthesis of methoxypoly(ethylene glycol) N-succinimidyl ester (MePEG-NHS)

In a 100 mL round bottom flask, MePEG-COOH (2.55 g, 1.28×10^{-3} mol) and *N*-hydroxysuccinimide (0.306 g, 2.67×10^{-3} mol) were dissolved in THF (40 mL). Afterwards, a solution of 4-dimethylaminopyridine (0.20 g, 1.64×10^{-3} mol) and *N,N* dicyclohexylcarbodiimide (0.53 g, 2.57×10^{-3} mol) in 2 mL of THF was introduced dropwise by a syringe. The reaction mixture was stirred during 18 h at room temperature under nitrogen atmosphere. After the reaction, the solid was filtered off and the THF was removed under reduced pressure. The solid was then recrystalized in 2-propanol and dried under high vacuum to give a fine, white powder in a quantitative fashion. ^{1}H NMR ($CDCl_3$) δ = 2.85 (s, 4H, $COCH_2CH_2CO$), 3.37 (s, 3H, OCH_3), 3.45–3.95 (m, 190H, OCH_2CH_2O), 4.51 (s, 2H, OCH_2CO).

2.4. PEGylation of Fe_3O_4–SiO_2–APTS nanocomposites

In a typical synthesis (**M01**), Fe_3O_4–SiO_2–APTS (10 mg) was suspended in anhydrous DMSO (3.8 mL) and TEA (0.2 mL, 5 vol.% with respect to DMSO), followed by the addition of MePEG-NHS (130 mg, 6.5×10^{-5} mol). The reaction mixture was then stirred for 24 h at room temperature. In order to remove unreacted MePEG-NHS and organic solvents, the solid was isolated by centrifugation (1000 rpm for 30 min at 20 °C) and dialysed against MilliQ® water (MilliQ® Ultrapure Water Purification System, Millipore) for 4 days using a membrane bag with a 12–14 kDa molecular weight cut-off. This was followed by three centrifugation/resuspension cycles in MilliQ® water. The water was then evaporated under reduced pressure and the sample was dried under high vacuum until constant weight. Sample **M02** was obtained under similar experimental conditions except that the reaction has been conducted following a 2.0-fold dilution regarding the Fe_3O_4–SiO_2–APTS nanocomposite.

2.5. Isothermal titration calorimetry (ITC) experiments

An isothermal calorimeter (VP-ITC, MicroCal Inc., USA) has been used to evaluate the interactions between bovine serum albumin (BSA), a model globular protein, and different nanocomposites synthesized in this work. The ITC instrument was periodically calibrated either electrically using an internal electric heater, or chemically by measuring the dilution enthalpy of methanol in water. This standard reaction was in excellent agreement (1–2%) with MicroCal constructor data (Othman et al., 2009; Segura-Sanchez et al., 2009). In a typical experiment, aliquots of 5 μL of BSA solution (5.4×10^{-2} mM) filled into a 283 μL syringe were used to titrate a suspension of nanocomposites (Fe_3O_4–SiO_2 or PEG-coated Fe_3O_4–SiO_2) at 0.605 mg mL^{-1} into the calorimetric cell accurately thermostated at 37 °C. Intervals between injections were 300 s and agitation speed was 394 rpm. Two backgrounds of titration consisted on injecting the BSA solution in solely MilliQ® water placed in the sample cell and injecting water into nanocomposites. The corresponding heat flow recorded as a function of time accounts for dilution effect.

2.6. Biocompatibility evaluation

2.6.1. Cell culture

In this work, human breast adenocarcinoma (MCF-7) and mouse macrophage (J774) cell lines were chosen for *in vitro* experiments. Both cell lines were grown in a humified atmosphere with 5% CO_2 at 37 °C. MCF-7 cells were grown in Dulbecco's modified Eagle's medium (Biowhittaker DMEM with 4.5 g L^{-1} glucose and L-glutamine, Lonza, Verviers, Belgium) supplemented with 10% fetal bovine serum, and 50 U mL^{-1} of penicillin and streptomycin. J774 cells were grown in RPMI-1640 medium (Biowhittaker with L-glutamine, Lonza, Verviers, Belgium) supplemented with 10% heat-inactivated fetal bovine serum, and 50 U mL^{-1} of penicillin and streptomycin.

2.6.2. In vitro cell viability studies

The MTT test is a quantitative colorimetric assay for the measurement of cell viability or cytotoxicity (Sgouras and Duncan, 1990). The 3-(4,5-dimethylthiazol-2-yl)-2,5-diphenyltetrazolium-bromide (MTT) is a yellow water-soluble tetrazolium salt converted to insoluble formazan crystals by active mitochondrial dehydrogenases of living cells. The MCF-7 cells (8000 cells per well) and the J774 cells (1000 cells per well) were seeded into 96 well plate and incubated with an aliquot of suspension containing nanocomposites at different concentrations (Fe_3O_4–SiO_2, Fe_3O_4–SiO_2–APTS or PEG-coated Fe_3O_4–SiO_2 nanocomposites) for 72 h. Then, 25 μL of a MTT solution (5 mg mL^{-1}) was added to each well and the incubation was carried out for 1.5 h. The medium was then removed and the converted dye was solubilized with 200 μL of DMSO. The absorbance of converted dye, which correlates with the number of viable cells, was measured at 570 nm, with subtraction of background absorbance at 650 nm, using a microplate reader (Labsystems multiskan MS, Thermo Electron, Les Ulis, France). The spectrophotometer was calibrated to zero absorbance using cell culture without nanocomposites.

2.6.3. Cellular uptake by in vitro Prussian Blue assay

Ferric ions react with potassium ferrocyanide to give a bright blue pigment called Prussian Blue. This assay was already used to highlight cellular uptake of nanocomposites (Schöpf et al., 2005). Briefly, MCF-7 cells (density of 2000 cells per mL) and J774 cells (density of 250 cells per mL) were seeded into Lab-Tek™ Chambered Coverglass (ATGC, Croissy-Beaubourg, France). After 24 h, cells were incubated with the particles suspension (at 10 μg mL^{-1} for Fe_3O_4–SiO_2 and 100 μg mL^{-1} for PEG-coated Fe_3O_4–SiO_2 nanocomposites) for 2 h at 37 °C. The medium was then removed and the cells were washed once with PBS, fixed with paraformaldehyde 2%, and incubated with a 10% solution of potassium ferrocyanide and a 20% aqueous solution of hydrochloric acid (1:1; v/v) for 20 min. Cells were then stained with Nuclear Fast Red (MM France, Francheville, France), where the nuclei were stained in red and the cytoplasm in pink, to investigate any change regarding cell morphology. After one washing, the slides were dehydrated, dried at room temperature and covered with a coverslip mounted

(Eukitt, CML, Montereau, France) prior observation using a Nikon inverse microscope (Nikon France, Champigny-sur-Marne, France).

2.7. Characterization techniques

The crystalline structure and morphology of samples were determined using X-ray powder diffraction (XRD) and transmission electron microscopy (TEM). The XRD spectra were collected by a Siemens D500 diffractometer with MoKα radiation, in the Bragg-Brentano geometry in the range $5 < 2\theta < 45^\circ$ with steps of 0.05° and a counting time of 16 s per step. Transmission electron microscopy observations were carried out using a JEOL CX200 (JEOL USA, Inc.) microscope operating at 200 kV. The sample was dispersed in octane in an ultrasonic bath and dropped onto a conventional carbon-coated copper grid. Fourier transform infrared spectroscopy (FT-IR) was used (Perkin Elmer FT-IR) to study the surface functionalization with MePEG-NHS. The FT-IR spectra were recorded in 600–4000 cm^{-1} region with KBr-pellet technique. Nanocomposites average diameter (D_z) was measured by dynamic light scattering (DLS) with a Nano ZS from Malvern (173° scattering angle) at a temperature of 25 °C. Aqueous electrophoresis data were obtained using the same apparatus. The zeta-potential (ζ) was calculated from the electrophoretic mobility (u) using the Smoluchowsky relationship $\zeta = \eta u/\varepsilon f(\kappa a)$, where it is assumed that $\kappa a \gg 1$ where η is the solution viscosity, ε is the dielectric constant of the medium, and κ and a are the Debye-Hückel parameter and the particle radius, respectively, $f(\kappa a)$ is the Henry's function and its value is 1.5 (Smoluchowski approximation) when the electrophoretic determinations of zeta potential are made in aqueous media and moderate electrolyte concentration. ζ-Potential measurements of dilute aqueous solutions of the nanocomposites were carried out at 25 °C in 10^{-3} M KCl. Prior analyses, samples of nanocomposites were resuspended in MilliQ® water and filtrated over 1 μm glass slide filters to removed aggregates.

3. Results and discussion

3.1. Synthesis and characterization of functionalized magnetite–silica nanocomposites

The Fe_3O_4–SiO_2 nanocomposites with 6 wt.% in SiO_2 were synthesized by the HEBM technique, starting from a mixture of Fe_2O_3 and Si powder. It has been generally described that during the milling process, the energy which is transferred from the balls to the powder leads both to the reduction of crystallite grain size and to a broad variety of defects such as cracks, new surfaces, mass transfer, etc. (Suryanarayana, 2001). The progressive dispersion and the intimate contact between elements give rise to a solid state reaction which, in our case, evolves to the formation of magnetite and silica as intermediate products (Corrias et al., 1997).

The evolution of the HEBM process was followed by XRD on withdrawn portions of sample at different milling time. After only 4 h of milling, characteristic magnetite diffraction peaks were observed in the XRD pattern where the indexing of electron diffraction pattern revealed the presence of magnetite as single crystalline phase (Fig. 1). In contrast, the SiO_2 amorphous phase gave rise to diffuse haloes without any diffraction peaks. From the XRD pattern *via* the Scherrer equation, the average crystallites size was estimated to be ~6 nm.

This result is in good agreement with TEM observations, which was performed under bright-field (BF) and dark-field (DF) imaging modes (Fig. 2). The bright field image revealed that the milling process produced aggregates of nanoparticles, the size of the latter ranging from approximately 100 to 200 nm (Fig. 2a). In the dark field mode, the sample appeared as bright, spherical magnetite

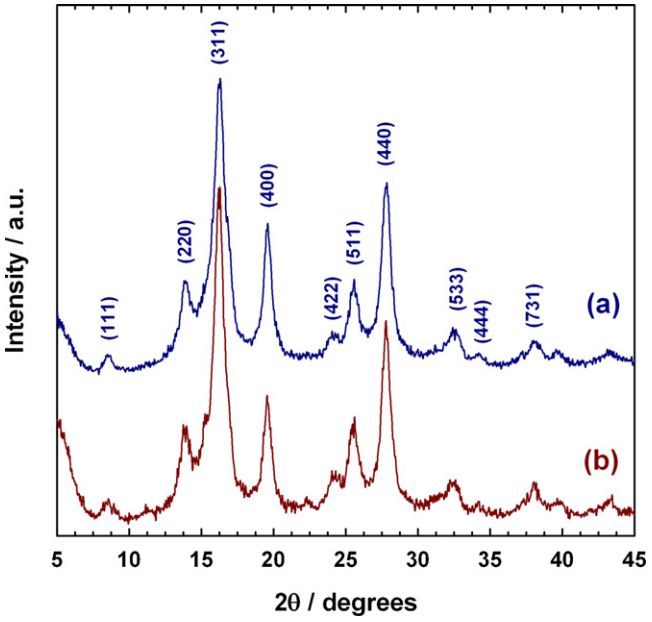

Fig. 1. XRD pattern of Fe_3O_4–SiO_2 (a) and Fe_3O_4–SiO_2–APTS (b) nanocomposites. Bragg peaks are indexed as magnetite according to JCPDS card no. 19-0629. For the main peaks, respective Miller indexes ($h\,k\,l$) are reported.

nanoparticles almost homogeneously dispersed into the amorphous matrix of silica (Fig. 2b). The selected area electron diffraction (SAED) pattern in Fig. 2c confirms the nanometric magnetite structure suggested by the XRD data.

In order to introduce amine functions at the surface of the nanocomposites for further coupling with reactive PEG, Fe_3O_4–SiO_2 nanocomposites were first derivatized with APTS *via* a silanization reaction (del Campo et al., 2005). This process comprised two steps. First, the organosilane and the nanocomposites were placed into an acidic aqueous solution where a silane polymer was obtained by concomitant hydrolysis and condensation reactions. In the second step, a covalent bond was formed between the silane polymer and Fe_3O_4–SiO_2 nanocomposites *via* hydroxyl groups (Brinker et al., 1990). Indeed, it is well-known that APTS can covalently bind either hydroxyl groups of metal oxide or silanol groups (Pham et al., 2007a,b; Yamaura et al., 2004), both present at the surface of the nanocomposites. The successful derivatization of Fe_3O_4–SiO_2 nanocomposites by APTS was shown by FT-IR spectroscopy (Fig. 3a). Fe_3O_4–SiO_2–APTS nanocomposites present two characteristic bands of NH_2 terminal groups at 3421 and 1625 cm^{-1} due to ν(N–H) stretching and bending vibration, respectively, in good agreement with the literature data (Mohapatra et al., 2007). The bands at 2930 and 2862 cm^{-1} are respectively assigned to ν_{as}(C–H) and ν_s(C–H) stretching vibration of APTS propyl groups. It is worth mentioning the presence of characteristic bands at 1130 and 1190 cm^{-1}, which correspond to ν(Si–O–Si) stretching (Jitianu et al., 2006), thus confirming the adsorption of the silane polymer at the surface of the nanocomposites.

Silanized nanocomposites (Fe_3O_4–SiO_2–APTS) exhibited similar XRD pattern than the one of Fe_3O_4–SiO_2 (Fig. 1b) where no appreciable shift in peaks position was evidenced. Besides, no magnetite crystallites grew up after silanization as observed in the average crystallites size calculated using the Scherrer equation which was still around 6 nm. Therefore, the positioning of APTS moieties at the surface of the Fe_3O_4–SiO_2 nanocomposites by the formation of Si–O–Si and Si–O–Fe bonds did not alter the structure of the resulting material which now displays primary amine groups available for further coupling reactions (Feng et al., 2008; Liu et al., 2004a).

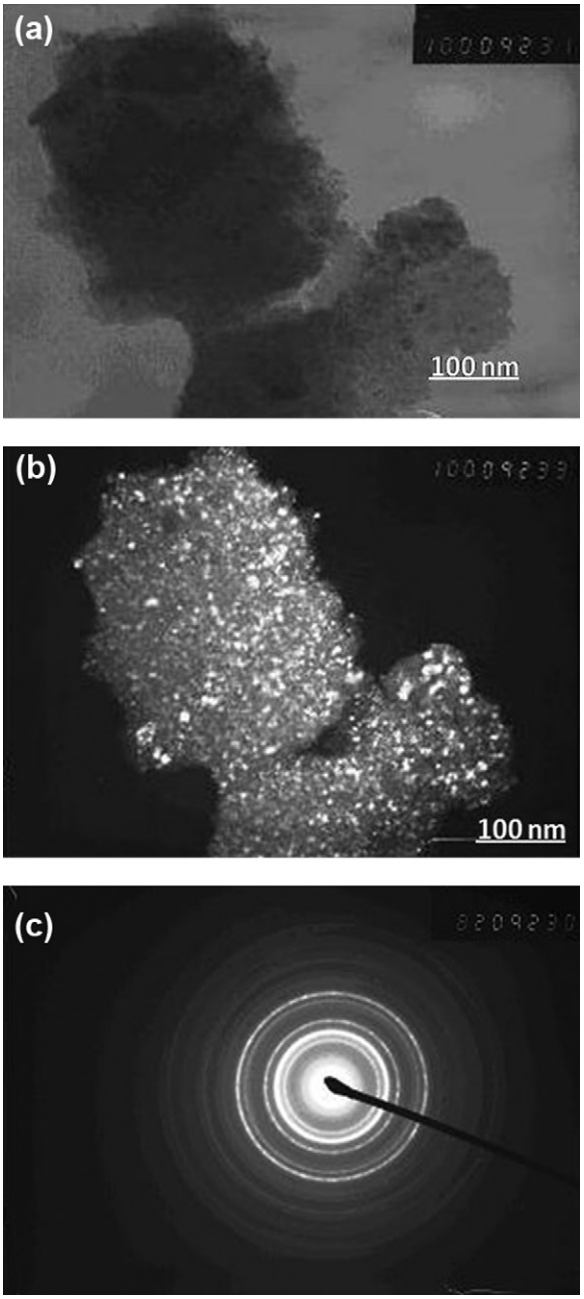

Fig. 2. Transmission electron micrographs of Fe_3O_4–SiO_2 nanocomposites collected after 4 h of milling: bright field image (a), dark field image (b) and selected area electron diffraction (SAED) pattern obtained with the Fe_3O_4–SiO_2 nanocomposites (c).

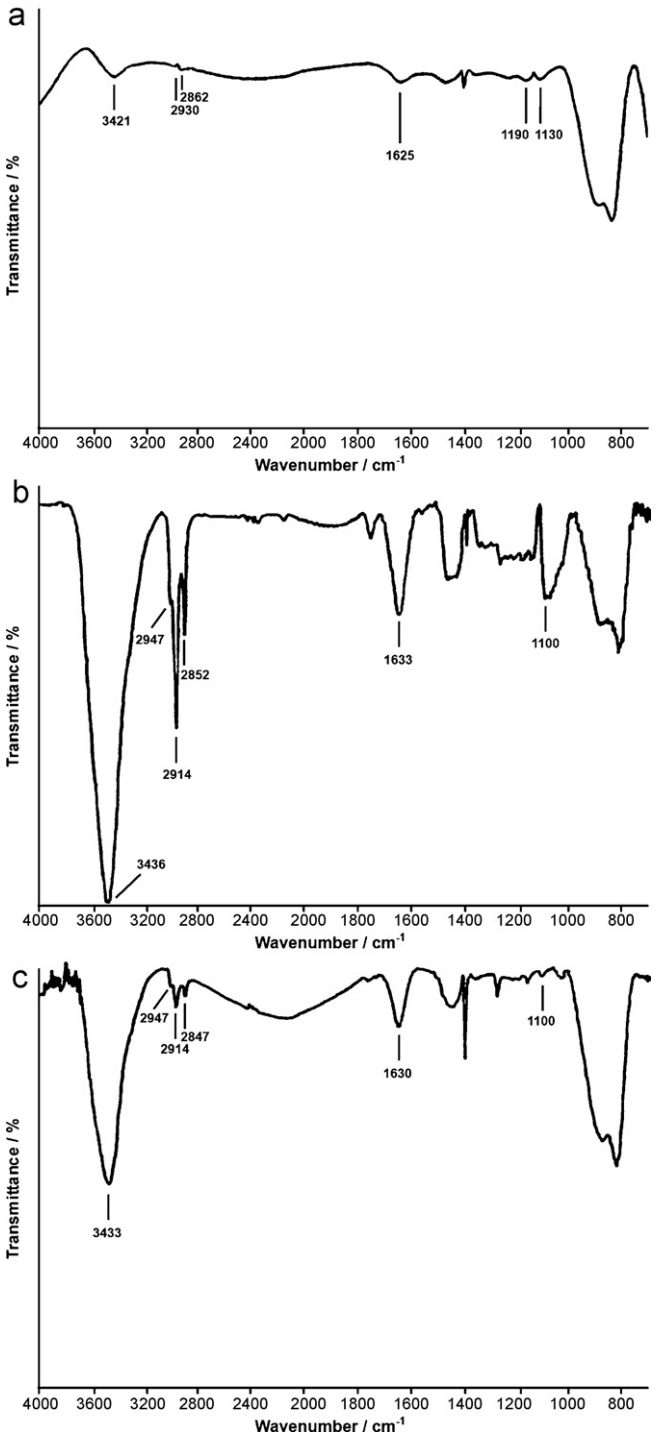

Fig. 3. Fourier transform infrared (FT-IR) spectra of Fe_3O_4–SiO_2–APTS nanocomposites (a), PEG-coated Fe_3O_4–SiO_2 nanocomposites **M01** (b) and **M02** (c).

3.2. PEGylation of magnetite–silica nanocomposites

In order to confer long-term colloidal stability and stealth properties to the nanocomposites, a PEGylation approach using methoxypoly(ethylene glycol) *N*-succinimidyl ester (MePEG-NHS) was investigated. The MePEG-NHS was expected to react with APTS amine moieties randomly displayed at the surface of Fe_3O_4–SiO_2–APTS nanocomposites *via* amide bonds formation. MePEG-NHS was synthesized following a two-step procedure from commercially available poly(ethylene glycol) monomethyl ether. First, the terminal hydroxyl group was converted into a carboxylic acid moiety by Jones oxidation followed by standard DCC coupling reaction with *N*-hydroxysuccinimide in a quantitative fashion (see experimental part). The PEGylation was then undertaken at ambient temperature for 24 h in a DMSO/TEA mixture in the presence of a suspension of Fe_3O_4–SiO_2–APTS nanocomposites. It yielded samples **M01** and **M02** which differed in the applied reaction conditions (see experimental part).

The coupling reaction was confirmed by FT-IR spectroscopy. Indeed, nanocomposites **M01** (Fig. 3b) exhibited a characteristic band at 1633 cm^{-1} of ν(amide C=O) stretching vibration (note that the ν(N–H) stretching vibration band at 3436 cm^{-1} is increased by remaining traces of water in the sample, usually observed due to the hygroscopic feature of PEG). The coating with PEG chains was

also proved by the bands at 2947, 2914 and 2852 cm^{-1}, respectively, assigned to ν_{as}(C–H) and ν(C–H) stretching vibration, and by a band at 1100 cm^{-1} characteristic of ν(C–O–C) stretching vibration (Xu et al., 2003). For the nanocomposites **M02** (Fig. 3c), analogous bands were obtained but with significantly lower intensities, hence demonstrating a higher PEGylation yield for **M01** compared to **M02**.

3.3. Colloidal characteristics of magnetite–silica nanocomposites

The aqueous suspensions of Fe_3O_4–SiO_2 and Fe_3O_4–SiO_2–APTS nanocomposites both conducted to the formation of large aggregates suffering from gravitational sedimentation after few days as evidenced by DLS. This may be due to the HEBM technique which does not allow the size and the particle size distribution to be finely tuned. Besides, even though the coupling of APTS should prevent magnetic interaction and hence particle aggregation, it has been shown on the basis of DLVO theory that a too high concentration of APTS resulted in a significant loss of colloidal stability (Mohapatra et al., 2007). This led to a relatively narrow window where optimal stability was observed, which is here quite difficult to reach according to the employed method to generate the nanocomposites. Nevertheless, PEGylation drastically improved colloidal characteristics to the nanocomposites. Indeed, PEGylated Fe_3O_4–SiO_2 nanocomposites **M01** and **M02** exhibited D_z = 200 and 314 nm together with reasonable particle size distributions (polydispersity indexes were 0.211 and 0.290, respectively). Noteworthy to mention is the large amount of micro-sized (~2.6 μm) particles obtained when Fe_3O_4–SiO_2–APTS nanocomposites were resuspended in a 10% aqueous solution of Pluronic F68. This could highlight the crucial role of the coupling with PEG chains rather than simple adsorption of a PEG-based surfactant to obtain nanocomposites with satisfying colloidal properties.

However, long-term stability studies of PEGylated nanocomposites were performed and revealed that sample **M02** conducted to partial sedimentation after several days, probably because of a less efficient PEG coverage, as expected from FT-IR spectroscopy results. In contrast, PEGylated Fe_3O_4–SiO_2 nanocomposites **M01** were perfectly stable with no sedimentation over time.

ζ-Potential measurement of nanocomposites **M01** was then performed as an indication of the repulsive force that is present and of their long-term stability. They exhibited negative ζ-potential values of -26.4 ± 2.3, which is in a suitable window for biomedical applications. For instance, PEGylated poly(alkyl cyanoacrylate) nanoparticles which are widely used for biomedical applications usually exhibit negative ζ-potentials around −20 mV (Brambilla et al., 2010; Kim et al., 2007).

3.4. Evaluation of protein interaction with PEGylated nanocomposites

Protein adsorption on nanoparticles is a crucial step towards the cellular transport and recognition mechanisms. In order to evaluate the ability of PEG-coated Fe_3O_4–SiO_2 nanocomposites to prevent protein adsorption and, therefore, to confirm the presence of PEG chains at the surface of nanocomposites, ITC was applied. Nowadays, ITC is becoming the method of choice for nanoparticles surface characterization with exquisite sensitivity, since the turbidity or the colour of the samples has no influence on the measurement (Bouchemal, 2008). Characterization was performed with non-PEGylated or PEGylated Fe_3O_4–SiO_2 nanocomposites and BSA, a model globular protein. BSA, which consists of 607 amino acids with 17 disulfide bonds and one free cysteine residue (Janatova et al., 1968), was selected as a model for human serum albumin. Besides, its structure comprises three repeating domains.

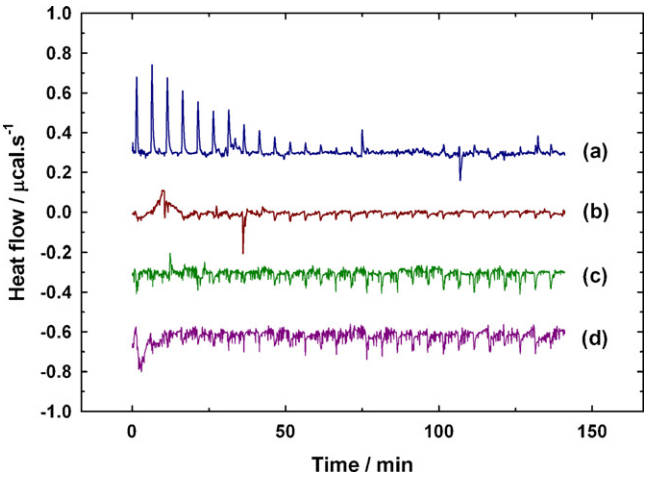

Fig. 4. Typical ITC thermograms corresponding to the titration of Fe_3O_4–SiO_2 nanocomposites (a) and PEGylated Fe_3O_4–SiO_2 nanocomposites **M01** (b) with BSA solution (5.4×10^{-2} mM). Controls consisted on the injection of BSA solution into MilliQ® water (c) and on the injection water into a suspension of Fe_3O_4–SiO_2 nanocomposites (d).

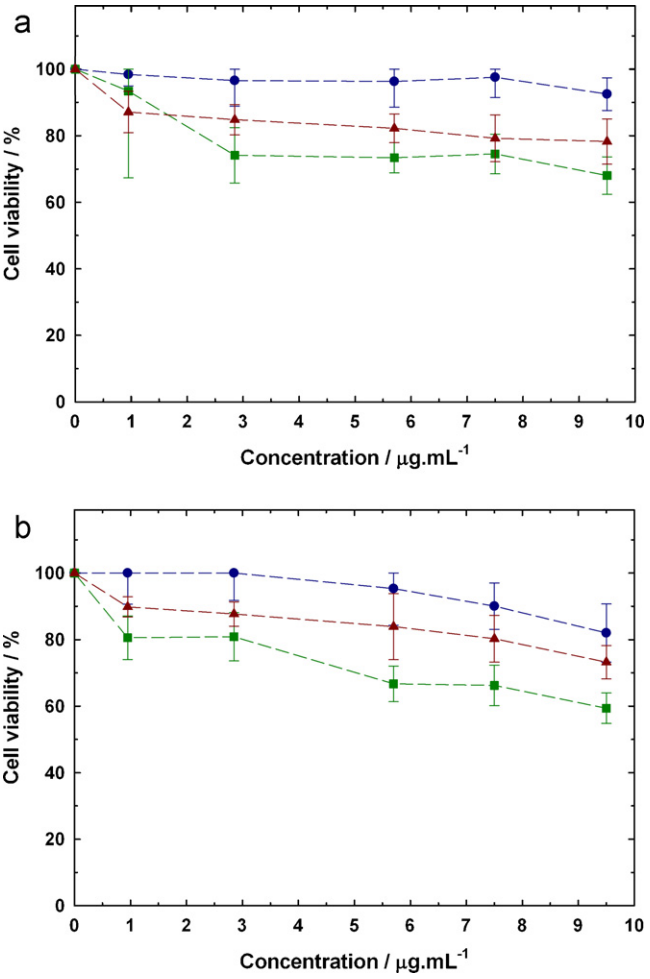

Fig. 5. Cell viability of MCF-7 breast cancer cells (a) and J774 macrophages cells (b) after exposure to various concentrations of Fe_3O_4–SiO_2 (●), Fe_3O_4–SiO_2–APTS (■) and PEG-coated Fe_3O_4–SiO_2 nanocomposites **M01** (▲) for 72 h. Each experiment was repeated eight times on 5 independent nanocomposite preparations. Results are expressed as percentages of absorption of treated cells (±SD) in comparison with the values obtained from untreated control cells.

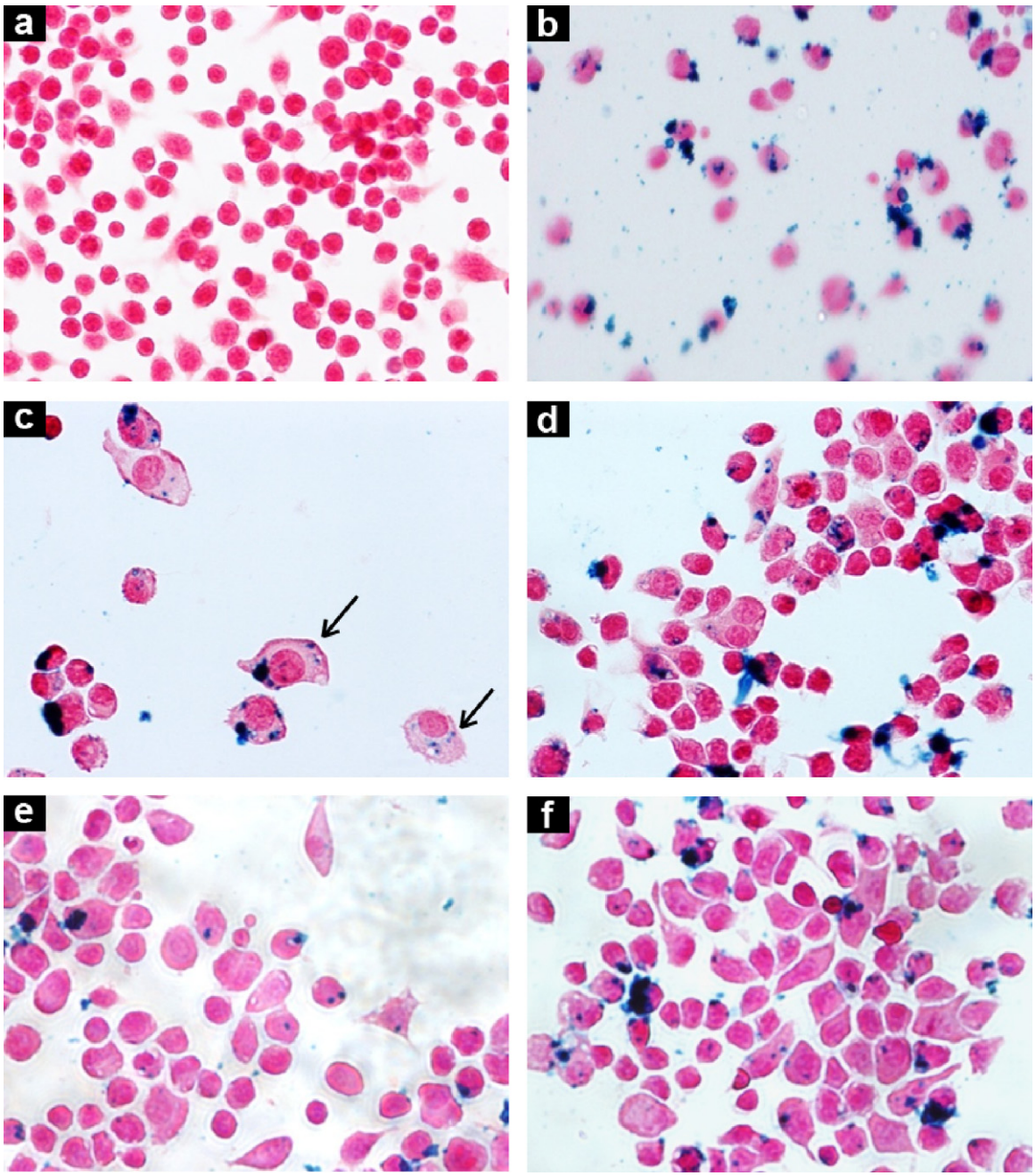

Fig. 6. Nanocomposite uptake with J774 cells following a 2 h incubation period (Prussian blue staining). Control (untreated) cells (a), cells incubated with Fe_3O_4–SiO_2 (b), PEG-coated Fe_3O_4–SiO_2 nanocomposites **M01** (c and d) and **M02** (e and f). Magnification: 20× (a and d); 40× (b, e and f) and 100× (c).

Hydrophilic residues are located on the protein surface, whereas hydrophobic ones are buried into the protein (Larsericsdotter et al., 2005).

Theoretically, PEG chains grafted at the surface of nanocomposites should ovoid, or at least reduce protein adsorption due to steric repulsions and hydrophilization. As shown in Fig. 4, ITC permitted to confirm the difference in the surface properties of these two kinds of magnetite–silica nanocomposites. ITC thermograms obtained with Fe_3O_4–SiO_2 nanocomposites (Fig. 4a) were indeed drastically different in comparison with the one corresponding to PEGylated Fe_3O_4–SiO_2 nanocomposites (Fig. 4b). Upon titration of Fe_3O_4–SiO_2 nanocomposites, endothermic peaks are initially observed subsequent to each injection. After 12 injections, a noticeable decrease in the peak intensities was observed and the heat flow remained fairly constant over time.

As a consequence, the peaks shown in Fig. 4a, characteristic of an endothermic process during the ITC experiment, were clearly assigned to the interactions between BSA and Fe_3O_4–SiO_2 nanocomposites. The presence of Fe_3O_4–SiO_2 nanocomposites in the reaction cell caused an appreciable change in enthalpy in comparison to controls consisting on the injection of a BSA solution into water (Fig. 4c) and on the injection of water into a suspension of Fe_3O_4–SiO_2 nanocomposites (Fig. 4d). However, when PEGylated Fe_3O_4–SiO_2 nanocomposites (**M01**) were titrated with a BSA solution, no change in the heat flow was observed. This revealed that PEGylated Fe_3O_4–SiO_2 nanocomposites did not interact with the protein due to efficient coverage by PEG chains.

However, interpretation of the observed endothermic process upon adsorption of BSA is not straightforward because it may result from a combination of various factors. It could be assigned to the

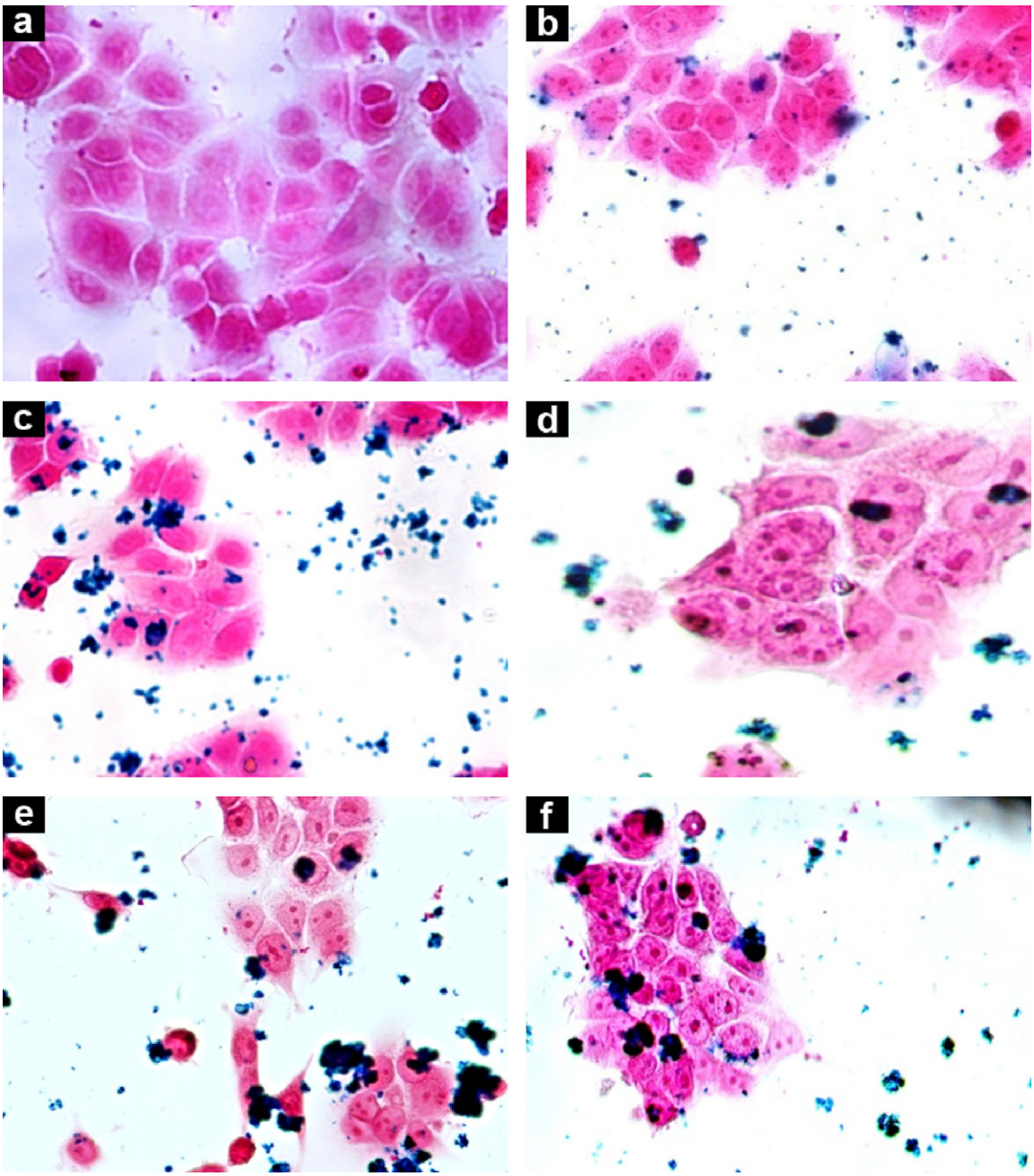

Fig. 7. Nanocomposite uptake with MCF-7 cells following a 2 h incubation period (Prussian blue staining). Control (untreated) cells (a), cells incubated with Fe_3O_4–SiO_2 (b), PEG-coated Fe_3O_4–SiO_2 nanocomposites **M01** (c and d) and **M02** (e and f). Magnification: 40× (e and f) and 100× (a–d).

presence of hydroxyl groups of silica. The presence of hydroxyl groups at the surface of Fe_3O_4–SiO_2 nanocomposites was confirmed by the highly negative ζ-potential value (-29.6 ± 2.7 mV at pH 6–7) in agreement with the literature data (Pham et al., 2007a,b; Yu et al., 2009). Besides, it was reported in a recent work that hydroxyl groups interact with BSA *via* hydrogen bonds formation and electrostatic interactions. However, it has been reported that a partial unfolding of secondary structures on the external sheath of the protein takes place due to competitive hydrogen bonding interactions of functional groups such as C=O and NH with surface acidic OH groups from silica (Yu et al., 2009). The endothermic process observed during titration of Fe_3O_4–SiO_2 may then be assigned to the formation of this unfolded BSA structure. For instance, it has been shown that interaction between BSA and negatively charged polystyrene surfaces led to structural changes of the protein and modification of its hydration state (Lynch and Dawson, 2008; Norde and Giacomelli, 2000).

3.5. Cytotoxicity studies

Cytotoxicity of Fe_3O_4–SiO_2, Fe_3O_4–SiO_2–APTS and PEG-coated Fe_3O_4–SiO_2 nanocomposites **M01** was estimated by standard MTT assay following a 72 h incubation period with J774 macrophages and MCF-7 breast cancer cells *via* a dose-dependence approach. From the results (Fig. 5), several important trends can be highlighted. First, no statistical difference in cytotoxicity was observed between Fe_3O_4–SiO_2 nanocomposites up to 10 μg mL^{-1} irrespective of the cell line. However, Fe_3O_4–SiO_2–APTS nanocomposites conducted to a significant decrease in the cell viability. This result is probably due to the presence of APTS amino groups attached to

the surface of the nanocomposites. Indeed, Petushkov et al. (2009) recently investigated cytotoxicity of silicalite nanoparticles with different crystal sizes and different surface functional groups. In their study, they showed that amine-functionalized nanoparticles in the 30–500 nm range exhibited a significant increase in toxicity with human embryonic kidney 293 (HEK-293) cells than other types of surface functionalization (i.e. thiol and carboxylic acid).

In contrast, when Fe_3O_4–SiO_2 nanocomposites were PEGylated, a very significant decrease of cytotoxicity leading to more than 80% cell viability even at the highest concentration was observed on both cell lines (Fig. 5). This is explained by the disappearing of surface amine groups in favor of amide bonds (upon PEGylation), even though cell viability was not as high as for uncoated Fe_3O_4–SiO_2 nanocomposites. This is probably due to: (i) remaining amine groups present at the surface of the nanocomposites and/or (ii) the internalization of the nanocomposites that may interfere with cell metabolism. Nevertheless, this significant increase in cell viability compared to the one observed with Fe_3O_4–SiO_2–APTS is another proof of the attachment of PEG chains at the surface of Fe_3O_4–SiO_2 nanocomposites.

The cellular uptake of Fe_3O_4–SiO_2 and PEG-coated Fe_3O_4–SiO_2 nanocomposites upon incubation with J774 (Fig. 6) and MCF-7 (Fig. 7) cell lines has been then qualitatively compared using Prussian blue staining. Noteworthy, after a 2 h incubation period with nanocomposites, nuclear fast red staining did not reveal neither any change in cellular morphology with both cell lines nor cell death, in good agreement with previously shown results regarding cell viability assays. Bright blue stained Fe_3O_4–SiO_2 nanocomposites as well as a small fraction of aggregates were detected and nanoparticles seemed to be mainly located in the extracellular compartment of the cells. However, when covered by PEG chains (Fig. 6c–f), the resulting nanocomposites seemed to be internalized into the cytoplasm of J774 cells (this observation was made on the basis of numerous images randomly taken from the cells monolayer). Interestingly, this sub-cellular localization was even more pronounced with **M01** nanocomposites (see arrows in Fig. 6c) which may be correlated to a better colloidal stability due to a higher PEGylation yield, hence preventing the formation of aggregates not suitable for being internalized by endocytosis.

Concerning the MCF-7 cell line, internalization of PEGylated Fe_3O_4–SiO_2 nanocomposites is far less visible (Fig. 7). This could be explained by the nature of the cells that are well-known to have a poor tendency for endocytosis compared to J774 cells. Indeed, such a kind of cell line is able to internalize solutes very rapidly taking in the equivalent of their cell volume every 2 h (Steinman et al., 1976; Swanson et al., 1985).

4. Conclusion

For the first time, PEGylated magnetite–silica nanocomposites intended to be used for biological purposes have been prepared by HEBM. This "solid state method" allowed the production of Fe_3O_4–SiO_2 nanocomposites further functionalized by APTS *via* a silanization process to introduce surface amine groups. The resulting nanocomposites were then PEGylated by MePEG-NHS to confer long-term colloidal stability and stealth properties.

By ITC, it was shown that non-PEGylated nanocomposites led to significant interaction with BSA, employed here as a model globular protein, whereas PEGylated nanocomposites did not interact with the protein due to efficient coverage by PEG chains. To the best of our knowledge, it is the first time that ITC was used to investigate surface functionalization of magnetite–silica nanocomposites and turned out to be a suitable and very sensitive method.

Cytotoxicity studies demonstrated that Fe_3O_4–SiO_2 and PEGylated Fe_3O_4–SiO_2 nanocomposites did not provide any significant cytotoxicity on J774 macrophage and MCF-7 breast cancer cell lines. This was shown by cell viability assays and cell morphology investigation. However, noticeable internalization was only evidenced with J774 cells and PEGylated Fe_3O_4–SiO_2 nanocomposites in contrast to MCF-7 cells for which no cellular uptake could be demonstrated, in good agreement with the nature of each cell line and especially with their respective tendency for endocytosis.

Even though this preliminary study is extremely encouraging and clearly showed the important potential of HEMB regarding the synthesis of PEG-coated Fe_3O_4–SiO_2 nanocomposites for biological purposes, some work remains to be done and should be focused on their surface functionalization with ligands of interest. Indeed, this is of crucial importance regarding active cell targeting in order to open the door to the so-called theranostic approach (i.e. nanomaterials allowing both diagnostic and therapy to be performed).

Acknowledgments

The authors thank Dr. Didier Desmaële for fruitful discussions. Fondazione Banco di Sardegna, CNRS and French Ministry of Research are warmly acknowledged for funding.

References

Barnakov, Y.A., Yu, M.H., Rosenzweig, Z., 2005. Manipulation of the magnetic properties of magnetite–silica nanocomposite materials by controlled stober synthesis. Langmuir 21, 7524.

Bouchemal, K., 2008. New challenges for pharmaceutical formulations and drug delivery system characterization using isothermal titration calorimetry. Drug Discov. Today 13, 960–972.

Brambilla, D., Nicolas, J., Le Droumaguet, B., Andrieux, K., Marsaud, V., Couraud, P.-O., Couvreur, P., 2010. Design of fluorescently tagged poly(alkyl cyanoacrylate) nanoparticles for human brain endothelial cell imaging. Chem. Commun. 46, 2602–2604.

Brinker, C., Scherer, G., 1990. Sol–Gel Science: The Physics and Chemistry of Sol–Gel Processing. Academic Press, Inc., New York, N.Y.

Butterworth, M.D., Bell, S.A., Armes, S.P., Simpson, A.W.J., 1996. Colloid Interface Sci. 183, 91.

Castrillo, P.D., Olmos, D., Amador, D.R., Gonzàlez-Benito, J., 2007. Real dispersion of isolated fumed silica nanoparticles in highly filled PMMA prepared by high energy ball milling. Polymer 308, 318–324.

Corrias, A., Ennas, G., Musinu, A., Paschina, G., Zedda, D., 1997. Iron-silica and nickel–silica nanocomposites prepared by high energy ball milling. J. Mater. Res. 12, 2767–2772.

del Campo, A., Sen, T., Lellouche, J.P., Bruce, I.J., 2005. Multifunctional magnetite and silica-magnetite nanoparticles: synthesis, surface activation and applications in life sciences. J. Magn. Magn. Mater. 293, 33–40.

Deng, Y.-H., Wang, C.-C., Hu, J.-H., Yang, W.-L., Fu, S.-K., 2005. Colloids Surf. A: Physicochem. Eng. Aspects 262, 87.

Di Marco, M., Sadun, C., Port, M., Guilbert, I., Couvreur, P., Dubernet, C., 2007. Physicochemical characterization of ultrasmall superparamagnetic iron oxide particles (USPIO) for biomedical application as MRI contrast agents. Int. J. Nanomed. 2, 609–622.

Feng, B., Hong, R.Y., Wang, L.S., Guo, L., Li, H.Z., Ding, J., Zheng, Y., Wei, D.G., 2008. Synthesis of Fe_3O_4/APTES/PEG diacid functionalized magnetic nanoparticles for MR imaging. Colloids Surf. A: Physicochem. Eng. Aspects 328, 52–59.

Gao, X., Yu, K.M.K., Tamb, K.Y., Tsang, S.C., 2003. Colloidal stable silica encapsulated nano-magnetic composite as a novel bio-catalyst carrier. Chem. Commun., 2998.

Im, S.H., Herricks, T., Lee, Y.T., Xia, Y., 2005. Synthesis and characterization of monodisperse silica colloids loaded with superparamagnetic iron oxide nanoparticles. Chem. Phys. Lett. 401, 19.

Ishida, T., Tamaru, S., 1993. Mechanical alloying of polymer/metal systems. J. Mater. Sci. Lett. 12, 1851–1853.

Janatova, J., Fuller, J.K., Hunter, M.J., 1968. The heterogeneity of bovine albumin with respect to sulfhydryl and dimer content. J. Biol. Chem. 243, 3612–3622.

Jitianu, A., Raileanu, M., Crisan, M., Predoi, D., Jitianu, M., Stanciu, L., Zaharescu, M., 2006. Fe_3O_4–SiO_2 nanocomposites obtained via alkoxide and colloidal route. J. Sol-Gel Sci. Technol. 40, 317–323.

Kim, H.R., Gil, S., Andrieux, K., Nicolas, V., Appel, M., Chacun, H., Desmaele, D., Taran, F., Georgin, D., Couvreur, P., 2007. Low-density lipoprotein receptor-mediated endocytosis of PEGylated nanoparticles in rat brain endothelial cells. Cell. Mol. Life Sci. 64, 356–364.

Kobayashi, Y., Saeki, S., Yoshida, M., Nagao, D., Konno, M., 2008. Synthesis of spherical submicron-sized magnetite/silica nanocomposite particles. J. Sol-Gel Sci. Technol. 45, 35–41.

Kong, L.B., Zhang, T.S., Ma, J., Boey, F., 2008. Progress in synthesis of ferroelectric ceramic materials via high-energy mechanochemical technique. Prog. Mater. Sci. 53, 207–322.

Larsericsdotter, H., Oscarsson, S., Buijs, J., 2005. Structure, stability, and orientation of BSA adsorbed to silica. J. Colloid Interface Sci. 289, 26–35.

Laurent, S., Forge, D., Port, M., Roch, A., Robic, C., Vander Elst, L., Muller, R.N., 2008. Magnetic iron oxide nanoparticles: synthesis, stabilization, vectorization, physicochemical characterizations, and biological applications. Chem. Rev. 108, 2064–2110.

Lele, B.S., Kulkarni, M.G., 1998. Single step room temperature oxidation of poly(ethylene glycol) to poly(oxyethylene)-dicarboxylic acid. J. Appl. Polym. Sci. 70, 883–890.

Liu, X., Ma, Z., Xing, J., Liu, H., 2004a. Preparation and characterization of amino-silane modified superparamagnetic silica nanospheres. J. Magn. Magn. Mater. 270, 1–6.

Liu, X., Xing, J., Guan, Y., Shan, G., Liu, H., 2004b. Colloids Surf. A: Physicochem. Eng. Aspects 238, 127.

Lu, Y., Yin, Y., Mayers, B.T., Xia, Y., 2002. Modifying the surface properties of superparamagnetic iron oxide nanoparticles through a Sol–Gel approach. Nano Lett. 2, 183.

Lynch, I., Dawson, K.A., 2008. Protein–nanoparticle interactions. Nanotoday 3, 1–2.

Mohapatra, S., Pramanik, N., Mukherjee, S., Ghosh, S.K., Pramanik, P., 2007. A simple synthesis of amine-derivatised superparamagnetic iron oxide nanoparticles for bioapplications. J. Mater. Sci. 42, 7566–7574.

Na, H.B., Song, I.C., Hyeon, T., 2009. Inorganic nanoparticles for MRI contrast agents. Adv. Mater. 21, 2133–2148.

Neuberger, T., Schöpf, B., Hofmann, H., Hofmann, M., von Rechenberg, B., 2005. Superparamagnetic nanoparticles for biomedical applications: possibilities and limitations of a new drug delivery system. J. Magn. Magn. Mater. 293, 483–496.

Norde, W., Giacomelli, C.E., 2000. BSA structural changes during homomolecular exchange between the adsorbed and the dissolved states. J. Biotechnol. 79, 259–268.

Othman, M., Bouchemal, K., Couvreur, P., Gref, R., 2009. Microcalorimetric investigation on the formation of supramolecular nanoassemblies of associative polymers loaded with gadolinium chelate derivatives. Int. J. Pharm. 379, 218–225.

Petushkov, A., Intra, J., Graham, J.B., Larsen, S.C., Salem, A.K., 2009. Effect of crystal size and surface functionalization on the cytotoxicity of silicalite-1 nanoparticles. Chem. Res. Toxicol. 22, 1359–1368.

Pham, K.N., Fullston, D., Sagoe-Crentsil, K., 2007a. Surface charge modification of nano-sized silica colloid. Aust. J. Chem. 60, 662–666.

Pham, K.N., Fullston, D., Sagoe-Crentsil, K., 2007b. Surface modification for stability of nano-sized silica colloids. J. Colloid Interface Sci. 315, 123–127.

Philipse, A.P., van Bruggen, M.P.B., Pathmamanoharan, C., 1994. Magnetic silica dispersions: preparation and stability of surface-modified silica particles with a magnetic core. Langmuir 10, 92.

Roberts, M.J., Bentley, M.D., Harris, J.M., 2002. Chemistry for peptide and protein PEGylation. Adv. Drug Deliv. Rev. 54, 459–476.

Sajja, H.K., East, M.P., Mao, H., Wang, Y.A., Nie, S., Yang, L., 2009. Development of multifunctional nanoparticles for targeted drug delivery and noninvasive imaging of therapeutic effect. Curr. Drug Discov. Technol. 6, 43–51.

Scano, A., Pilloni, M., Paschina, G., Ennas, G., submitted for publication. Meccanosynthesis, characterization and functionalization of Fe_3O_4/SiO_2 nanocomposites. J. Nanoparticles Res.

Schöpf, B., Neuberger, T., Schulze, K., Petri, A., Chastellain, M., Hofmann, M., Hofmann, H., von Rechenberg, B., 2005. Methodology description for detection of cellular uptake of PVA coated superparamagnetic iron oxide nanoparticles (SPION) in synovial cells of sheep. J. Magn. Magn. Mater. 293, 411–418.

Segura-Sanchez, F., Bouchemal, K., Lebas, G., Vauthier, C., Santos-Magalhaes, N.S., Ponchel, G., 2009. Elucidation of the complexation mechanism between (+)-usnic acid and cyclodextrins studied by isothermal titration calorimetry and phase-solubility diagram experiments. J. Mol. Recognit. 22, 232–241.

Sgouras, D., Duncan, R., 1990. Methods for the evaluation of biocompatibility of soluble synthetic polymers which have potential for biomedical use: 1. Use of the tetrazolium-based colorimetric assay (MTT) as a preliminary screen for evaluation of in vitro cytotoxicity. J. Mater. Sci.: Mater. Med. 1, 61–68.

Solinas, S., Piccaluga, G., Morales, M.P., Serna, C.J., 2001. Sol–gel formation of gamma-Fe_2O_3/SiO_2 nanocomposites. Acta Mater. 49, 2805–2811.

Sorrentino, A., Gorrasi, G., Tortora, M., Vittoria, V., Costantino, U., Marmottini, F., Padella, F., 2005. Incorporation of Mg–Al hydrotalcite into a biodegradable Poly([epsilon]-caprolactone) by high energy ball milling. Polymer 46, 1601–1608.

Steinman, R.M., Brodie, S.E., Cohn, Z.A., 1976. Membrane flow during pinocytosis. A stereologic analysis. J. Cell Biol. 68, 665–687.

Stöber, W., Fink, A., Bohn, E., 1968. Controlled growth of monodisperse silica spheres in the micron size range. J. Colloid Interface Sci. 26, 62.

Stolnik, S., Illum, L., Davis, S.S., 1995. Long circulating microparticulate drug carriers. Adv. Drug Deliv. Rev. 16, 195–214.

Sun, Y., Duan, L., Guo, Z., DuanMu, Y., Ma, M., Xu, L., Zhang, Y., Gu, N., 2004. An improved way to prepare superparamagnetic magnetite–silica core-shell nanoparticles for possible biological application. J. Magn. Magn. Mater. 285, 65–70.

Suryanarayana, C., 2001. Mechanical alloying and milling. Prog. Mater. Sci. 46, 1–184.

Swanson, J.A., Yirinec, B.D., Silverstein, S.C., 1985. Phorbol esters and horseradish peroxidase stimulate pinocytosis and redirect the flow of pinocytosed fluid in macrophages. J. Cell Biol. 100, 851–859.

Tartaj, P., Serna, C.J., 2002. Microemulsion-assisted synthesis of tunable superparamagnetic composites. Chem. Mater. 14, 4396.

Tartaj, P., Serna, C.J., 2003. Synthesis of monodisperse superparamagnetic Fe/silica nanospherical composites. J. Am. Chem. Soc. 125, 15754.

Teja, A.S., Koh, P.-Y., 2009. Synthesis, properties, and applications of magnetic iron oxide nanoparticles. Prog. Cryst. Growth Charact. Mater. 55, 22–45.

Veronese, F.M., 2001. Peptide and protein PEGylation. A review of problems and solutions. Biomaterials 22, 405–417.

Veronese, F.M., Harris, J.M., 2002. Introduction and overview of peptide and protein pegylation. Adv. Drug Deliv. Rev. 54, 453–456.

Xu, H., Yan, F., Monson, E.E., Kopelman, R., 2003. Room-temperature preparation and characterization of poly(ethylene glycol)-coated silica nanoparticles for biomedical applications. J. Biomed. Mater. Res. 66, 870–879.

Yamaura, M., Camilo, R.L., Sampaio, L.C., Macêdo, M.A., Nakamura, M., Toma, H.E., 2004. Preparation and characterization of (3-aminopropyl)triethoxysilane-coated magnetite nanoparticles. J. Magn. Magn. Mater. 279, 210–217.

Yu, C.H., Al-Saadi, A., Shih, S.J., Qiu, L., Tam, K.Y., Tsang, S.C., 2009. Immobilization of BSA on silica-coated magnetic iron oxide nanoparticle. J. Phys. Chem. C 113, 537–543.

Zhu, Y.G., Li, Z.Q., Zhang, D., Tanimoto, T., 2006. Abs/iron nanocomposites prepared by cryomilling. J. Appl. Polym. Sci. 99, 501.